行政院國家科學委員會專題研究計畫　期中進度報告

旋轉窯焚化爐中廢輪胎熱裂解反應動力參數分析及流場模擬之研究(2/3)

計畫類別： 個別型計畫
計畫編號： NSC92-2211-E-002-060-
執行期間： 92 年 08 月 01 日至 93 年 07 月 31 日
執行單位： 國立臺灣大學生物產業機電工程學系暨研究所

計畫主持人： 吳中興

計畫參與人員： 楊凱元

報告類型： 精簡報告

處理方式： 本計畫可公開查詢

中　華　民　國 93 年 5 月 31 日

旋轉窯焚化爐中廢輪胎熱裂解反應動力參數分析及流場模擬之研究（2/3）

The Kinetic Parameters Analysis and Flow Field Simulations on Pyrolysis of Waste Tire Using a Rotary Kiln (2/3)

計畫編號：NSC92-2211-E-002-060　　　執行期間：2003.08.01-2004.07.31

計畫主持人：吳中興 國立台灣大學生物產業機電工程學系暨研究所

中文摘要：

本實驗並採用計算流體力學軟體 FLUENT 之有限體積分析法，解析使用廢輪胎延伸燃料（TIRE DERIVED FUEL）之工業用高雄市東南水泥廠逆向式旋轉窯焚化爐窯體內之熱流場、向量場、與物質反應的偏微分方程式，以反應操作模式中燃燒所需之過剩空氣量與溫度、旋轉爐之旋轉速度為主要參數，模擬燃燒氣體熱流場與旋轉窯壁之熱傳模式。其中燃燒模式為標準 k-ε 紊流模式。模擬結果與實際現場量測所得之溫度數值作相互比對，以進行各不同之燃燒反應參數在流場顯影之探討。

本實驗之溫度模擬結果與實際量測溫度具有良好之相關性：

燒成帶之溫度模擬變化值由 1550℃ 至 1640℃，而實驗之量測結果為介於 1450℃ 與 1540℃；窯體外殼量測溫度介於 200℃ 與 350℃ 之間；窯尾之溫度量測值與實驗數值亦分別為 1050℃ 與 850℃ 至 1200℃ 之範圍內。誤差範圍為 9.25±2.8%。

根據數值模擬結果，窯體中之主要燃燒氣體溫度為 1450℃，且最終的排氣內含物質也依據實驗取得。並利用 ELPI、DM(DUST MONITOR)以及 GC 進行水泥廠廢氣所含 PM 與 PAH 的量測。實驗最後並利用電腦輔助工程軟體進行下一步之熱流場廢熱工程回收利用之預測。

英文摘要：

This study simulates a counter flow cement industry rotary kiln in Kaohsiung, Taiwan via computational fluid dynamics with finite volume method. The detailed properties of waste tire-derived-fuel are surveyed and adopted in the numerical studies with commercially available code FLUENT by standard k-ε turbulence and two-step methane combustion model. Partial differential equations of flow field are solved with PISO model with the dependent matrix of excess air, rotary/conferential speed. The simulated temperature in the sintering zone and the interior entity along the furnace body are depicted 1550-1640°C and 1450-1550°C, respectively. The exhaust gas is then collected and analyzed by ELPI, DM and GC to study the PM and PAHs content in cement process. The CAE simulated temperature contours are adopted for further analysis of waste heat recycling research.

關鍵字：

計算流體力學 (CFD)，有限體積法 (FVM)，FLUENT，廢輪胎延伸燃料（TDF），旋轉窯 (RKI)，電腦輔助工程(CAE)、ELPI（Electrical Low-Pressure Impactors）、DM（Dust Monitor）

計畫源由與目的：

A rotary kiln is a constructive incinerator widely used for treating industrial and hazardous waste. Owing to the operating properties of the temperature between 1200-1450°C and 5-10 seconds of residence time, it is broadly used all over the world (e.g. by America, Canada, France, Japan and Taiwan) to deal with the hazardous industrial wastes. This study investigated a 75 meter long industrial suspension-preheated cement rotary kiln in Kaohsiung, Taiwan, which is 3 degrees inclined and rotates at the rate of 0.3665 rad/s. Its detailed descriptions are shown in the following Figure 1 and Table 1:

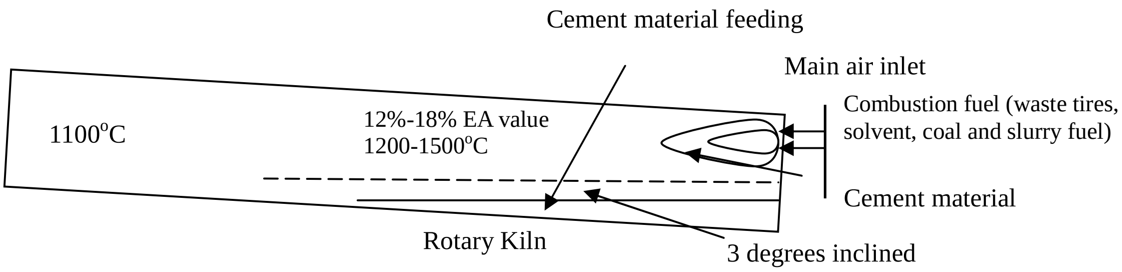

Figure 1. Schematic of the cement rotary kiln in Kaohsiung

Table 1. Physical descriptions of the rotary kiln

Dimensions of the kiln furnace (m)	
Length	75.0
Diameter	4.6
The angle of inclination (degree)	3.0
Rotating rate of the kiln furnace (r.p.m.)	3.7
Kiln shell thickness (with firebrick)	0.35
Relevant operating parameters	
Equivalent ratio	0.725-0.68
Feeding rate of raw material (kg/hr)	220800
Producing rate of the cement (kg/hr)	133800
Kiln head HHV (kcal)	6780
SHC (kcal/hr)	741
Residence time (sec)	6-10
Kiln temperature (°C)	1100-1550
Dioxin discharge (ng-TEQ/Nm3)	0.038-0.304

Before fueling for the kiln torch, a series of gasification process are previously applied to transfer the solid, liquid and slurry fuels into a mixture of syngas. The total gas phase carbon heat value in the kiln head area is acquired to be 741 kcal/ kg-clinker, which equals 3.1 MJ/kg clinker or 1.018×108 kcal/hr. With this, methane-air two-step reaction is introduced and the stoichiometric properties of the combustion are previously obtained and computed as table 2. At present 15% excess air operation, the detailed values of velocity and mass fractions of CH_4 and O_2 are listed within.

Table 2. Detailed stoichiometric properties of 15% excess air boundary condition

Equivalence Ratio	Mass Fraction_CH_4	Mass Fraction_O_2	Velocity of torch	Velocity of secondary air
0.69	0.066	0.215	48.59	1.001

In this rotary kiln, various fuel sources are adopted for the fire torch and the detailed ultimate analysis of the waste tire derived fuel is depicted as table 3.

For this, total heat value presents in kiln heat area can be computed as 6780 kcal as shown in Table 1 together with the composition of the fuel sources and this outcome of computation provides important clues for the boundary conditions further in numerical simulation.

Table 3. Ultimate analysis of sedan and truck waste tires

Ultimate analysis (%)	Sedan	Truck
Carbon	81.14	85.16
Hydrogen	7.22	7.42
Oxygen	2.07	1.72
Nitrogen	0.47	0.31
Sulfur	1.64	1.52
Chlorine	0.02	0.03
Physical composition (%)		
Moisture	0.54	0.87
Ash	5.73	4.54
Combustible	93.73	94.59
Experimental heat values		
HHV (kcal/kg)	8519.73	8129.86
LHV (kcal/kg)	7824.80	7537.89

結果與結論

In this study, the geometric and stoichiometric information of the rotary kiln are previously obtained to construct the physical schemes and grid mesh. All numerical and chemical manipulation properties are to be required and computed previously in order to study the mathematical parameters for simulation.

The temperature variation in the flame area is directly obtained by a pre-installed infrared temperature detector. In order to obtain more temperature comparisons for simulation, another temperature value on sampling position in the tail of the kiln is obtained to be 1015°C by a temperature data-logger acquisition system (21X, Campbell, Co. Ltd). In sintering zone, an infrared temperature sensor (POLCID-DC, KRUPP-POLYSIUS, Germany) located 5 meters inside the torch position is used to monitor the temperature variation continuously in 8 hours.

In this research of rotary kiln simulation, the heat flow field distribution has been visualized to study the interior heat flow patterns. The introduced numerical grid distributions of the interior physical domain and the kiln shell schematic are shown as following figures 2—304203 tetrahedral cells are generated and 432 triangular outlet faces are form in the interface between rotary kiln body and the pre-heater.

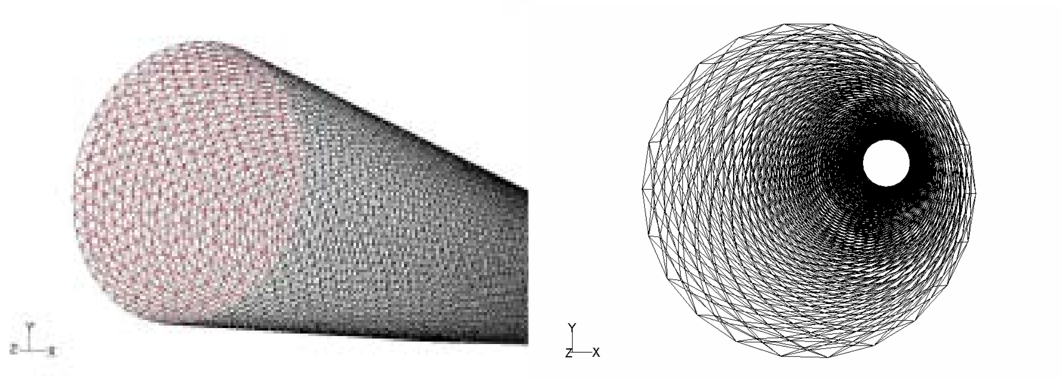

Figure 2. Schematic grid of the interior physical domain and the kiln shell entity

To study the shell conduction condition, further shell grid with 0.3 meters thick is then constructed outside this 75m long, 4.6m diameter furnace body. To complete the numerical construction, Nusselt number and the rotating conferential speed of kiln shell is derived to be 47.224 and 0.134 m/s, respectively. Heat transfer coefficient is then computed as 6.78 W/m2K for the natural convection on the outer surface of kiln shell by Gnielinski's equation. Figure 3 shows the experimental shell temperature variation along the kiln body from head to tail—these results are obtained via a sliding (BA-30TA, OPTEX Co. Ltd, Japan) and a portable infrared thermal detector (WI53224, Standard Equipment Co. Ltd) along the kiln body for correlating further simulations.

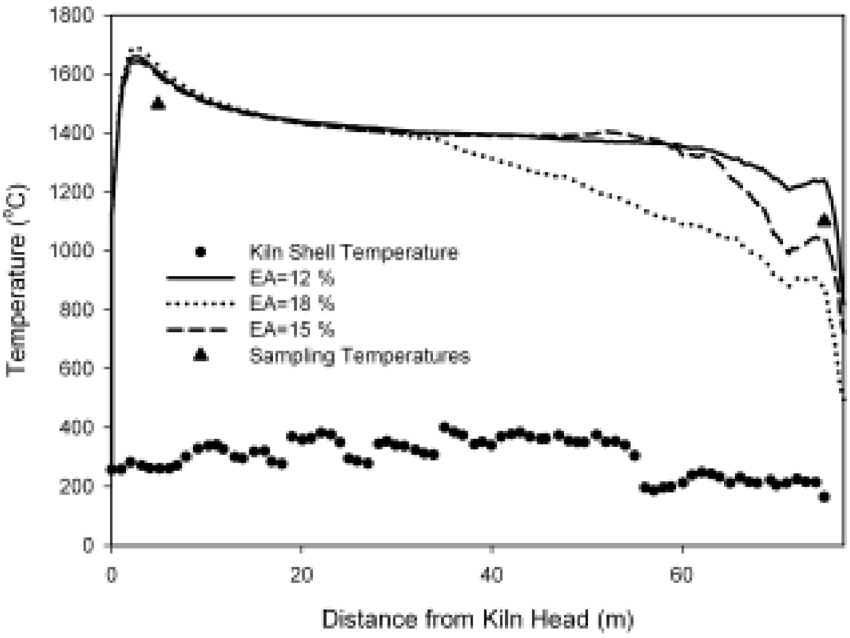

Figure 3. The kiln shell and interior gas temperature variation along the furnace experimentally and numerically

The simulated temperatures along the central axis of the rotary kiln with EA values from 12% to 18% are predicted numerically and are compared with experimental sampling temperatures in the cement sintering zone and kiln tail (triangular points). For that the detailed temperature information inside the furnace is impossible to access experimentally, numerically predicted temperature variation is then conducted by correlating the two sampling temperatures. The temperature variations along the kiln shell, inside the kiln body are also depicted experimentally as figure 3. This simulated temperatures of EA=15% correlates well with that in the released cement data book to raise in the kiln head area and drop gradually along the furnace body before temperature sink happens when main stream enters the pre-heater zone.

The production of cement also accompanies great amount of aerosol particulates that exist in transportation pipes and exhaust gas. On account of biological reasons, particles less than 3 μm easily enter the pulmonary alveolus regions thus cause asthma and other fatal diseases. The analysis of the exhaust particulate properties—especially the diameter distribution, therefore, is extremely important. With this, the studies of diameter distribution and number concentration are more important than that of mass concentration in the case of cement industry. According the relating EPA regulations in Taiwan, however, fixed pollution sources only have to meet certain standards of mass concentration and the novel literatures concerning cement industry have only done in way of particle mass concentrations. In this paper, studies of the exhaust gas of the cement industry in Kaohsiung, Taiwan are done with the methodology of aerosol analysis. ELPI (Electrical Low-Pressure Impactors, Dekati Ltd. Finland) and Dust Monitor (GRIMM, Germany) are introduced to examine the particle size between 0.075 μm-10 μm. The diameter distribution and number concentrations of the emitted aerosol are also studied accordingly.

Figure 4 shows the number concentration of size of particulates inside the exhaust. The main interception diameter lies in stage 8 is 1.0 μm and the mean diameter is 1.3 μm. In stage 2, the interception diameter is 0.06μm and the mean diameter is 0.081 μm while the number densities are 4000/cm3 and 3000/cm3. The geometric standard difference of distribution of size of exhaust's interior GSD is 3.264 and CMD is 0.415 μm.

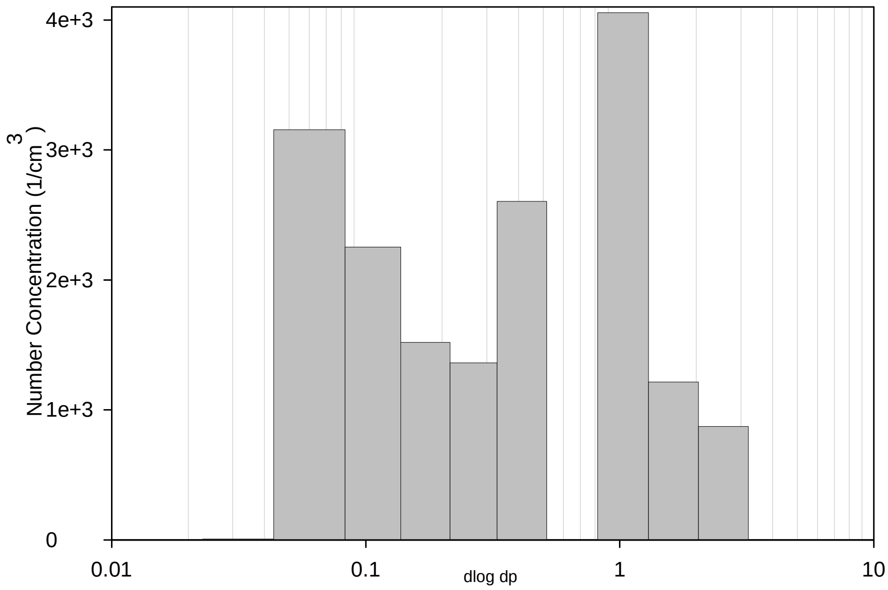

Figure 4. The number concentration of particulate size in the interior of exhaust tube

Figure 5 shows the number concentration of size of particulates in the entrance of the exhaust. The main interception diameter lies in stage 8 is 1.0 μm and the mean diameter is 1.3 μm. In stage 2, the interception diameter is 0.06 μm and the mean diameter is 0.081 μm. In stage 3, the interception diameter is 0.108 μm and the mean diameter is 0.14 μm while the number densities are 2500/cm3 and 1800 /cm3. The geometric standard difference of distribution of size of entrance of exhaust GSD is 2.832 and CMD is 0.322 μm.

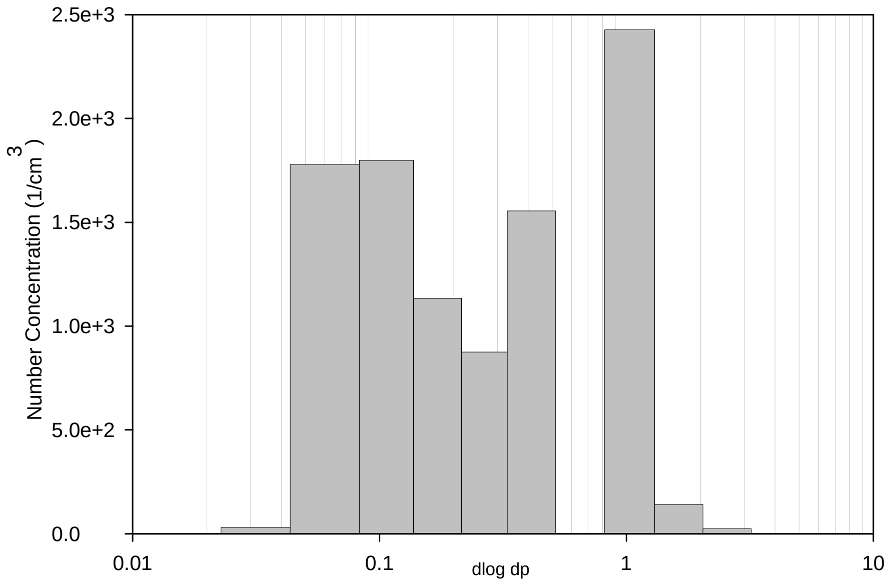

Figure 5. The number concentration of particulate size in the entrance of exhaust tube

Figure 6 shows the distribution of particulate size in atmosphere. The main size in atmosphere lies in stage 3 and is 0.108 μm and the mean size is 0.14 μm while the number density is 1200 /cm3. The geometric standard difference of distribution of size of atmosphere particulate is GSD=1.04 and CMD is 0.1437 μm.

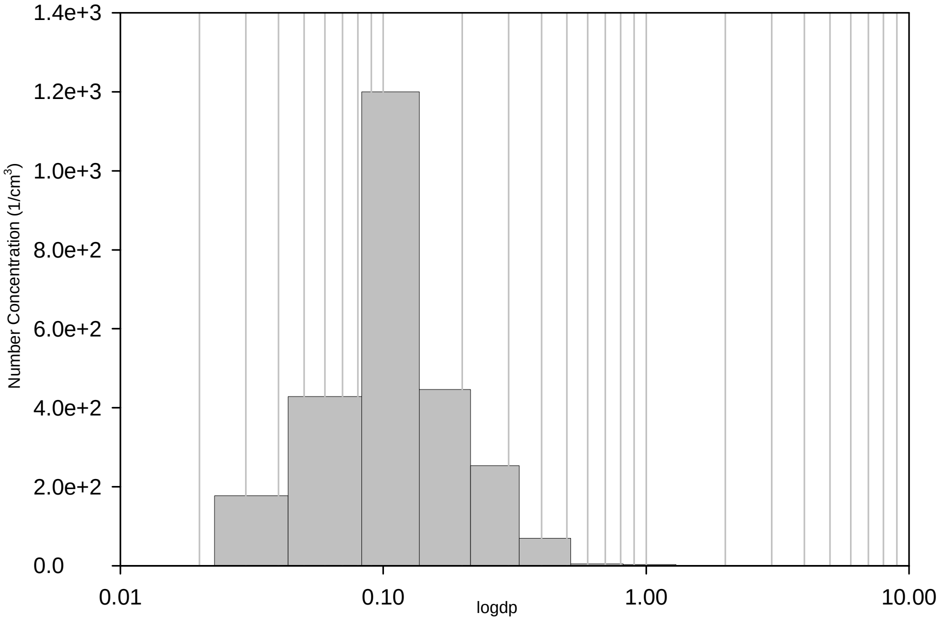

Figure 6. The number concentration of particulate size in atmosphere

The composition and properties of the exhaust are in Table 4. The exhausted matter is mainly NO_X. According to the comparison of ELPI of distribution of particulate size in atmosphere and inside and outside of the exhaust tube, we can get a mixed graph in Figure 7.

Table 4. The compositions and properties of gases in exhaust

Temperature in the exhaust	96oC
O2	14.2 %
CO	2773 ppm
NO	1230 ppm
NO2	4.8 ppm
NOx	1235 ppm
CO2	4.98 %

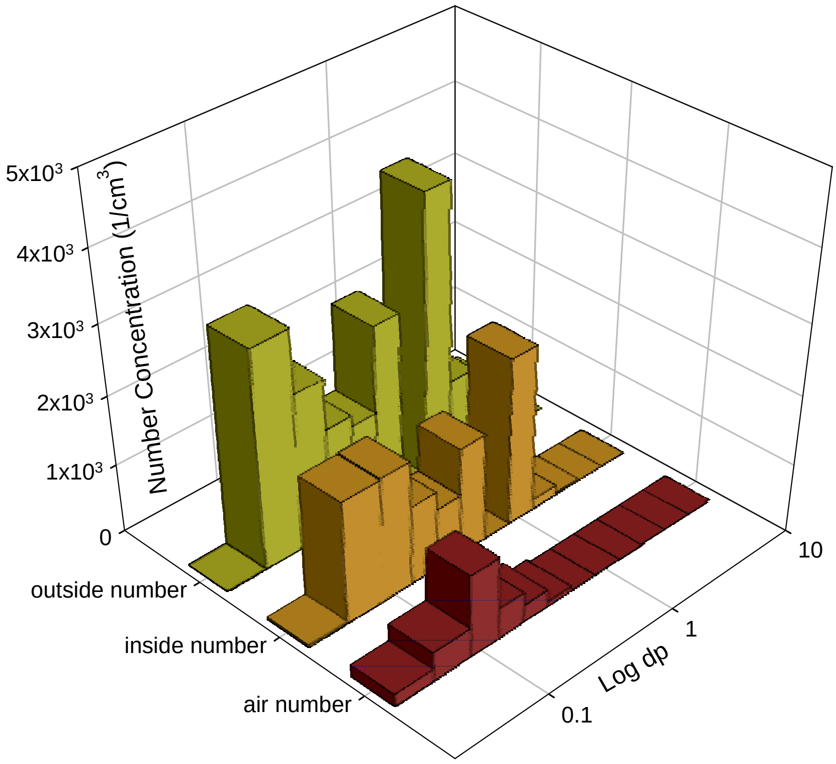

Figure 7. Comparison of the size of particulates inside and outside the exhaust tube

From Figure 8 and Table 5, we can also know the distributions of particulate size and PAHs emission in the interior of the exhaust tube and the sampling entrances are very close. However, while the size of particulate is bigger than 1.3 μm, the number density in the entrance of the tube drops a lot because of the gravity which makes bigger particulates adhered on the tube wall and causes the loss in statistics.

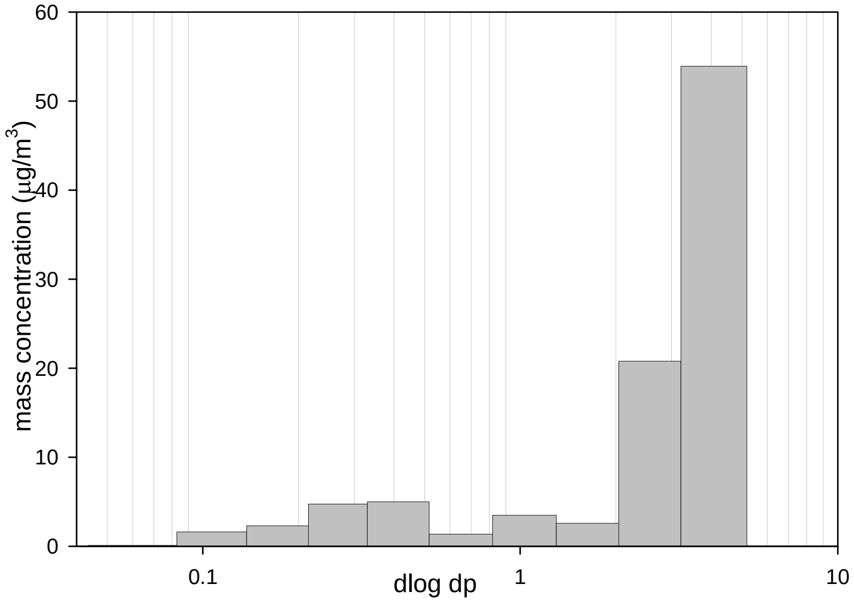

Figure 8. Mass concentration of particulate size in atmosphere

Table 5. The PAHs emission in the exhaust of cement process

Compound name	Molecular formula	PAHs Conc. (ng/m3)
Naphthalene	C10H8	0.296
Acenaphthylene	C12H8	0.688
Acenaphthene	C12H10	0.244
Fluerene	C13H10	0.633
Phenanthrene	C14H10	83.13
Anthracene	C14H10	1.384
Fluoranthene	C16H10	372.334
Pyrene	C16H10	3.658
Benzo(a)anthracene	C18H12	25.53
Chrysene	C18H12	24.59
Benzo(b)fluoranthene	C20H12	2.83
Benzo(k)fluoranthene	C20H12	4.97
Benzo(a)pyrene	C20H12	0.60
Indeno(123-cd)pyrene	C22H12	2.26
Dibenzo(ah)anthracene	C22H14	1.081
Benzo(ghi)perylene	C22H12	0.663

參考資料

Andrea, P. O., D. S. Itamar, J. M. Genesio and D. S. Rogerio Jose. 1998. Efficiency of destruction of waste used in the co-incineration in the rotary kilns. Energy Conversion Management. 39: 1899-1909.

Bahr, B., O. J. Hanssen, and M. Vold. 2003. Experiences of environmental performance eval- uation in the cement industry. Data quality of environmental performance indicators as a limiting factor for Benchmarking and Rating. Journal of Cleaner Production 11: 713-725.

Caretto, L.S., A.D. Gosman, S.V. Patankar and D.B. Spalding. 1972. Two calculation procedures for steady, three-dimensional flows with recirculation. Proc. 3rd. Int'l Conference on Numerical Methods for Fluid Mechanics. Lecture Notes on Physics, Springer-Verlag: New York. 19: 60-68.

Chen, K. S. and M. Lee. 1995. Visualization studies of three dimensional flow and solid motion in a rotary kiln. Hazardous waste and hazardous materials. 12(4): 395-409.

Cundy, V. A. and C. A. Cook, 1996. Three dimensional numerical modeling of a field-scale rotary kiln incinerator. Environmental Science and Technology.

Dekati. ELPI User Manual. Dekati Ltd. Tampere, Finland.

El-Banhawy, Y.H., Siv-Asegaram, S. 1983. Premixed, turbulent combustion of a sudden-expansion flow. Combustion and Flame. 80: 153-165.

Hinds, W. C. 1999. Aerosol Technology-Properties, Behavior, and Measurement of Airborne Particles, 2nd Ed. New York: John Wiley. 235-242.

International Commission on Radiological Protection. 1994. Human Respiratory Tract Model for Radiological Protection. Annals of the ICRP. Publication 66. Tarrytown, New York: Elsevier Science.

Irvine, J.T.S. and A. Sauve. 2001. Improved oxidation of hydrocarbons with new electrodes in high temperature fuel cell. Fuel Cells. 1(34): 205-210.

Khan, J. A., D. Pal and J. S. Morse. 1993. Numerical modeling of a rotary kiln incinerator. Hazardous Waste and Hazardous Materials. 10: 81-95.

Kramker, F. A. and J. B. Wilson. 1986. Computer simulation of a rotary dryer Part II: Heat and Mass Transfer. AIChE. 32(2): 269-275.

Lewis, M. H. and L. D. Smoot. 1982. Turbulent gaseous combustion and flame. 42: 183-196.

Mastorakos, E. et al. 1999. CFD prediction for cement kilns including flame modeling, heat transfer and clinker chemistry. Applied Mathematical Modeling. 23: 55-76.

Patankar, S.V. and D.B. Spalding. 1972. A calculation procedure for heat, mass, and momentum transfer in three-dimensional parabolic flows. International J. Heat Mass Transfer. 15: 1787-1806.

Pershing, D. W., J. S. Lighty, G. D. Silcox, M. P. Heap and W. D. Owens. 1993. Solid waste incineration in rotary kilns. Combustion Science and Technology. 93: 245-276.

Prodjosantoso, A. K. and B. J. Kennedy. 2003. Heavy metals in cement phases on the solubility of Mg, Cd, Pb and Ba in Ca3Al2O6. Cement and Concrete Research 33: 1077– 1084.

Silcox, G. D., F. S. Larsen and D. W. Pershing. 1990. Mathematical and physical modeling of rotary kilns with application to scaling and design. Incineration of Hazardous Waste and Toxic Combustion By-products.

Skvara, F., F. Kastanek, and I. Pavelkova. 2002. Solidification of waste steel foundry dust with Portland cement. Journal of Hazardous Materials. B89: 67–81.

Spalding, D.B. 1971. Mixing and chemical reaction in steady confined turbulent flames. 13th International Symposium on Combustion: The Combustion Institute. 649-657.

Veranth, J. M., G. D. Silcox and D. W. Pershing. 1997. Numerical modeling of the temperature distribution in a commercial hazardous waste slagging rotary kiln. Environmental Science and Technology. 31: 2534-2539.

Walter, H. D. 1976. Cement-Data-Book. Bauverlag GmbH Wiesbaden und Berlin. 336

Zaim, K. K. 1996. Emissions Due to Fossil-Fuel Consumption And Cement Production in Turkey (1970-1991). Energy. 21(4):325-331.